Experimental damage detection of wind turbine blade using thin film sensor array

Austin Downey[a], Simon Laflamme[a,b], Filippo Ubertini[c] and Partha Sarkar[d]

[a]Department of Civil, Construction, and Environmental Engineering, Iowa State University, Ames, IA, USA;
[b]Department of Electrical and Computer Engineering, Iowa State University, Ames, IA, USA;
[c]Department of Civil and Environmental Engineering, University of Perugia, Perugia, Italy;
[d]Department of Aerospace Engineering, Iowa State University, Ames, IA, USA;

ABSTRACT

Full Abstract

Damage detection of wind turbine blades is difficult due to their large sizes and complex geometries. Additionally, economic restraints limit the viability of high-cost monitoring methods. While it is possible to monitor certain global signatures through modal analysis, obtaining useful measurements over a blade's surface using off-the-shelf sensing technologies is difficult and typically not economical. A solution is to deploy dedicated sensor networks fabricated from inexpensive materials and electronics. The authors have recently developed a novel large-area electronic sensor measuring strain over very large surfaces. The sensing system is analogous to a biological skin, where local strain can be monitored over a global area. In this paper, we propose the utilization of a hybrid dense sensor network of soft elastomeric capacitors to detect, localize, and quantify damage, and resistive strain gauges to augment such dense sensor network with high accuracy data at key locations. The proposed hybrid dense sensor network is installed inside a wind turbine blade model and tested in a wind tunnel to simulate an operational environment. Damage in the form of changing boundary conditions is introduced into the monitored section of the blade. Results demonstrate the ability of the hybrid dense sensor network, and associated algorithms, to detect, localize, and quantify damage.

Keywords: structural health monitoring, capacitive-based sensor, soft elastomeric capacitor, flexible membrane sensor, sensor network, signal decomposition, damage detection, damage localization.

1. INTRODUCTION

A wind farm's economic viability typically relies on public subsidies, a predictable energy source, and reliable technologies.[1] The economic rewards of wind energy projects are particularly challenging due to the unpredictable operation and maintenance (O&M) costs. Reduction in the uncertainty related to the O&M costs of a wind turbine structural system[2] and the enabling of prognostics and health management (PHM)[3,4] is of interest to wind farm owners and operators. A key challenge to the PHM of a wind turbine blade is the implementation of a structural health monitoring (SHM) system that is cost effective and capable of distinguishing between local and global faults over the wind turbine's structural system.[5] This task is made more difficult for wind turbine blades due to their large sizes and complex geometries.[6] Implementation of an SHM system for wind turbine blades is further impeded by the high cost of traditional sensing systems.[2,5,6]

Cost effective monitoring solutions for wind turbine blades, in addition to other mesoscale (very large) structures, need to be capable of monitoring the structure's global (e.g., changing load paths, loss in global stiffness) and local (e.g., crack propagation) conditions. However, distinguishing between localized and global faults on a mesoscale system using state-of-the-art sensing technologies and practices is difficult.[7] In the case

Further author information: (Send correspondence to Austin Downey)
Austin Downey: E-mail: adowney2@iastate.edu

Sensors and Smart Structures Technologies for Civil, Mechanical, and Aerospace Systems 2017,
edited by Jerome P. Lynch, Proc. of SPIE Vol. 10168, 1016815 · © 2017 SPIE
CCC code: 0277-786X/17/$18 · doi: 10.1117/12.2261531

of wind turbine blades, SHM is further complicated by environmental effect (e.g temperature and humidity) on sensor signals.[8]

A solution to the global/local condition monitoring problem is the placement of dense sensor networks (DSNs) over the structure's global area, or at locations of interest.[2] Several innovative techniques for DSNs have emerged in recent years, including: distributed sensor arrays,[9,10] conductive paints,[11,12] and sensing skins.[13–17] In particular, Xu et al.[9] developed a 36-node sensor array of resistive heating elements built into a flexible polyimide film to measure flow separation on the leading edge of a delta-wing structure during wind tunnel tests. Tung et al.[14] presented a quantitative study on the relationship between crack growth and thermal variations for the characterization and future deployment of thin-film full-bridge strain sensors deployed on a polyimide sheet to form a DSN. Hallaji et al.[11] developed a large-area sensing skin consisting of electrically conductive copper paint for damage detection in concrete structures. Damage was detected and localized in the substrate through monitoring changes in the conductivity of the skin that is applied to the surface of the concrete. Loh et al.[15] introduced a carbon nanotube nanocomposite sensing skin that, when combined with electrical impedance tomography mapping, enabled two-dimensional damage detection and localization.

Within the same framework of DSNs, the authors have developed a soft elastomeric capacitor (SEC) designed for monitoring of mesoscale systems. The proposed SEC is a large area electronic that is inexpensive and simple to fabricate. The SEC is characterized by a parallel plate capacitor and was developed around an inexpensive nanocomposite based on a styrene-co-ethylene-co-butylene-co-styrene (SEBS) block co-polymer matrix. The SEBS matrix is filled with titania to form the sensor's dielectric, while the conductive electrodes consist of a SEBS matrix filled with carbon black. The SEC is customizable in shape and size,[17] and its static[18] and dynamic behaviors[5,19] have been characterized, including damage detection applications in wind turbine blades.[20] Its capability to detect fatigue cracks[21] and localize them within a DSN configuration[22] has been demonstrated.

The SEC offers the unique ability to measure the additive in-plane strain of a surface. Algorithms have been developed for the decomposition of the additive strain field into linear strain components along two orthogonal directions provided that certain boundary conditions are known or can be accurately assumed. Wu et al.[23] presented an algorithm designed to leverage a DSN configuration and a prescribed shape function with assumed boundary conditions to enable strain field decomposition. The algorithm used a least squares estimator (LSE) to fit linear strain components using the prescribed shape function, assuming the validity of the classical Kirchhoff plate theory. Numerical simulations demonstrated that a DSN of SECs could be used to reconstruct the unidirectional strain maps of a monitored surface. The work was further extended through the introduction of resistive strain gauges (RSGs) into the DSN to form a hybrid dense sensor network (HDSN) were the RSGs are used to enforce the algorithms boundary conditions.[24] Experimental validation showed that the HDSN was capable of reconstructing the unidirectional strain maps for a simply supported plate with an HDSN consisting of 20 SECs and a varying number of RSGs. The problem of RSG sensor location within the HDSN was addressed by Downey et al.[25] A genetic algorithm with a learning gene pool was used to obtain a 34.5% improvement in the fit of the strain maps when compared with the best fit from a best-of-50 initial guess.

This work presents a damage detection technique that is capable of damage detection and localization for a damage present along the edge of an HDSN consisting of SECs and RSGs. Here, the assumed boundary conditions are leveraged for damage detection, where changes in the boundary conditions are used to track damage in the monitored surface. Unidirectional full-field strain maps are reconstructed from the HDSN sensor data and the measured error between the reconstructed strain fields and the RSG sensors is used quantify the reconstructed strain maps. The level of error as a function of changing boundary conditions is monitored, and damage can be detected by minimizing the measured error. Results from an experimental investigation of an HDSN mounted inside the model of a wind turbine blade experiencing turbulent airflow in a wind tunnel are used for validation of the proposed technique. The HDSN consists of an array of 12 SECs and 8 RGSs.Damage in the form of changing boundary conditions along the edge of the monitored area is introduced into a fiberglass skin attached to the wind turbine blade.

The contributions of this work are two-fold: 1) demonstrate the ability of the SEC to monitor the model's global vibration characteristics in the relativity noisy environment of a wind tunnel; and 2) demonstrate that unidirectional strain maps extracted from an HDSN can be used for damage localization through the selection of proper boundary conditions. The paper is organized as follows. First, the background on the SEC sensor in

introduced, along with the strain decomposition algorithm. Second, the test methodology for the experimental validation is presented, which includes the algorithm formulation specialized for the model wind turbine blade. Third, a validation of the HDSNs capability to detect and localize damage through the updating of assumed boundary condition is presented. Finally, a summary of the results concludes the paper.

2. BACKGROUND

In this section, the background on the SEC sensor, including its electro-mechanical model and the previously developed extended LSE algorithm, is presented.

2.1 Soft Elastomeric Capacitor

The SEC is a robust and highly elastic large area electronic that transduces a change in a monitored substrate's geometry (i.e., strain) into a measurable change in capacitance. The sensor's fabrication,[17] static[18] and dynamic[5,19] characterization have been previously reported and are summarized here for completeness. The sensor's dielectric is composed of a styrene-ethylene-butylene-styrene (SEBS) block co-polymer matrix filled with titania to increase both its durability and permittivity. Additionally, its conductive plates are fabricated from the same SEBS, but filled with carbon black particles. Components used in the fabrication are readily available and its fabrication process is relatively simple, making the technology highly scalable.

The SEC measures the additive in-plane strain ($x-y$ plane in Figure 1(a)) of a monitored substrate. The SEC is pre-stretched and adhered to the substrate using commercial two-part epoxy. The SEC can be modeled as a non-lossy capacitor, assuming a low sampling rate (< 1 kHz), the with capacitance C given by the parallel plate capacitor equation,

$$C = e_0 e_r \frac{A}{h} \tag{1}$$

where $e_0 = 8.854$ pF/m is the vacuum permittivity, e_r is the polymer relative permittivity, $A = d \cdot l$ is the sensor area of width d and length l, and h is the thickness of the dielectric as annotated in Figure 1(a).

Assuming that the monitored substrate experiences only small strains, an expression relating the sensor's change in capacitance to the signal can be expressed as

$$\frac{\Delta C}{C} = \lambda(\varepsilon_x + \varepsilon_y) \tag{2}$$

where $\lambda = 1/(1-\nu)$ represents the gauge factor of the sensor, with ν being the sensor material's Poisson ratio. For SEBS, $\nu \approx 0.49$, which yields a gauge factor $\lambda \approx 2$. The electro-mechanical model is derived in reference.[5] Equation (2) shows that the signal of the SEC varies as a function of the additive strain $\varepsilon_x + \varepsilon_y$. The linearity of the derived electro-mechanical model holds for mechanical responses up to 15 Hz.[5] An altered electro-mechanical model has been derived for modeling mechanical responses up to 40 Hz,[19] but is not shown here for brevity. The SEC's electro-mechanical model has been validated at numerous occasions for both static[17,18,24] and dynamic[5,19] strain.

2.2 Strain Decomposition Algorithm

The extended LSE algorithm was designed to decompose the SEC signal's additive strain measurement, as expressed in Equation (2), by leveraging an HDSN configuration. The algorithm requires the knowledge of boundary conditions that can be either assumed[23] or enforced through the measurement of strain at key locations.[24] The extended LSE algorithm is presented in reference,[24] diagramed in figure 1(b), and summarized in what follows.

The extended LSE algorithm starts by assuming a p^{th} order polynomial displacement shape function. A polynomial function is selected as the displacement shape function due to its mathematical simplicity and its ability to develop a wide range of displacement topographies. The shape with a deflection function (w) is developed for the x-y plane such that

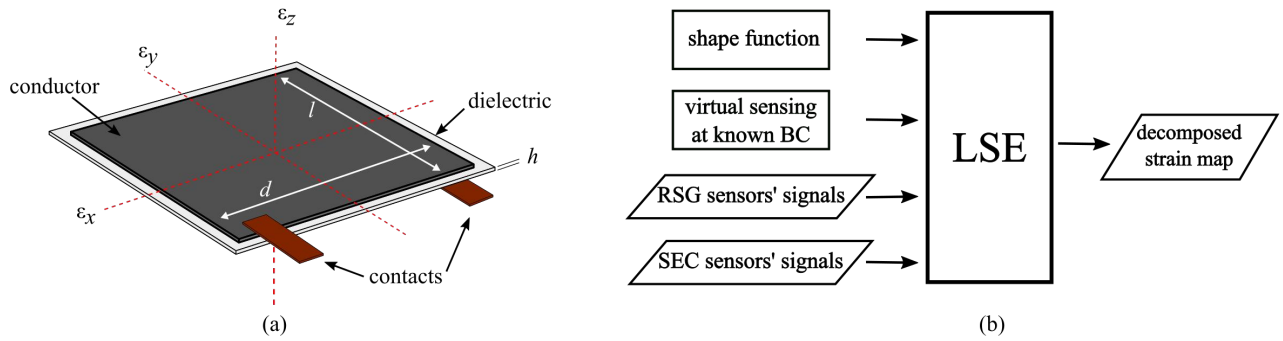

Figure 1. HDSN technology: (a) annotated SEC sensor with reference axes; and (b) extended LSE algorithm for developing unidirectional strain maps from an HDSN.

$$w\left(x,y\right)=\sum_{i=1,j=1}^{p}b_{ij}x^{i}y^{j} \tag{3}$$

where $b_{i,j}$ are regression coefficients. Considering an HDSN with m sensors that includes both SEC and RSG sensor nodes, displacements at the location of sensors are collected in a vector $\mathbf{W}$ such that $\mathbf{W}\in\mathbb{R}^{m}$. Eq. (3) becomes $\mathbf{W}=\left[\begin{array}{cccc} w_1 & \cdots & w_k & \cdots & w_m \end{array}\right]^{T}=\mathbf{HB}$, where subscript k is associated with the k-th sensor. Here, $\mathbf{H}$ contains the sensor locations and $\mathbf{B}$ contains the regression coefficients such that $\mathbf{B}=\left[\begin{array}{ccc} b_1 & \cdots & b_f \end{array}\right]^{T}$ for f regression coefficients.

The location matrix $\mathbf{H}$ is defined as $\mathbf{H}=[\mathbf{\Gamma}_{\mathrm{x}}\mathbf{H}_{\mathrm{x}}|\mathbf{\Gamma}_{\mathrm{y}}\mathbf{H}_{\mathrm{y}}]$ where $\mathbf{H}_{\mathrm{x}}$ and $\mathbf{H}_{\mathrm{y}}$ account for the SEC's additive strain measurements. $\mathbf{\Gamma}_x$ and $\mathbf{\Gamma}_y$ are diagonal weight matrices holding the scalar sensor weight values $\gamma_{x,k}$ and $\gamma_{y,k}$. For instance, an RSG sensor k orientated so that it measures strain in the x direction will take the weight values $\gamma_{x,k}=1$ and $\gamma_{y,k}=0$. Additionally, virtual sensors are used to enforce boundary conditions. Virtual sensors are treated as RSG sensors with known signals, typically $\varepsilon=0$, and are added into $\mathbf{H}$ at locations where the boundary condition can be assumed to a high degree of certainty. The matrices are developed from Equation (3);

$$\mathbf{H}_{\mathrm{x}}=\mathbf{H}_{\mathrm{y}}=\left[\begin{array}{ccccc} y_1^n & x_1y_1^{n-1} & \cdots & x_1^{n-1}y_1 & x_1^n \\ y_k^n & x_ky_k^{n-1} & \cdots & x_k^{n-1}y_k & x_k^n \\ y_m^n & x_my_m^{n-1} & \cdots & x_m^{n-1}y_m & x_m^n \end{array}\right] \tag{4}$$

Unidirectional strain functions ε_x and ε_y oriented along the x and y directions can be obtained from Equation 3 through the enforcement of Kirchhoffs plate theory as;

$$\varepsilon_x(x,y)=-\frac{c}{2}\frac{\partial^2 w(x,y)}{\partial x^2}=\mathbf{\Gamma}_{\mathrm{x}}\mathbf{H}_{\mathrm{x}}\mathbf{B}_{\mathrm{x}} \tag{5}$$

$$\varepsilon_y(x,y)=-\frac{c}{2}\frac{\partial^2 w(x,y)}{\partial y^2}=\mathbf{\Gamma}_{\mathrm{y}}\mathbf{H}_{\mathrm{y}}\mathbf{B}_{\mathrm{y}} \tag{6}$$

where $\mathbf{B}=[\mathbf{B}_{\mathrm{x}}|\mathbf{B}_{\mathrm{y}}]^{T}$, and c is the thickness of the plate.

A signal vector $\mathbf{S}$ is constructed from the measurements $\mathbf{S}=\left[\begin{array}{ccccc} s_1 & \cdots & s_k & \cdots & s_m \end{array}\right]^{T}$ were $s_k=\varepsilon_x+\varepsilon_y$ for an SEC and $s_k=\varepsilon_x$ or ε_y for a RSG. Thereafter, the regression coefficient matrix $\mathbf{B}$ can be estimated using an LSE:

$$\hat{\mathbf{B}} = (\mathbf{H}^T\mathbf{H})^{-1}\mathbf{H}^T\mathbf{S} \tag{7}$$

where the hat denotes an estimation. It results that the estimated strain maps can be reconstructed using

$$\hat{\mathbf{E}}_{\mathrm{x}} = \mathbf{\Gamma}_{\mathrm{x}}\mathbf{H}_{\mathrm{x}}\hat{\mathbf{B}}_{\mathrm{x}} \qquad \hat{\mathbf{E}}_{\mathrm{y}} = \mathbf{\Gamma}_{\mathrm{y}}\mathbf{H}_{\mathrm{y}}\hat{\mathbf{B}}_{\mathrm{y}} \tag{8}$$

where $\hat{\mathbf{E}}_{\mathrm{x}}$ and $\hat{\mathbf{E}}_{\mathrm{y}}$ are vectors containing the estimated strain in the x and y directions for sensors transducing $\varepsilon_x(x, y)$ and $\varepsilon_y(x, y)$, respectively.

An HDSN without a sufficient number of enforced boundary conditions will result in $\mathbf{H}$ being multi-collinear because $\mathbf{H}_{\mathrm{x}}$ and $\mathbf{H}_{\mathrm{y}}$ share multiple columns, resulting in $\mathbf{H}^T\mathbf{H}$ being non-invertible. This can be avoided by integrating a sufficient number of RSGs into the HDSN.

3. METHODOLOGY

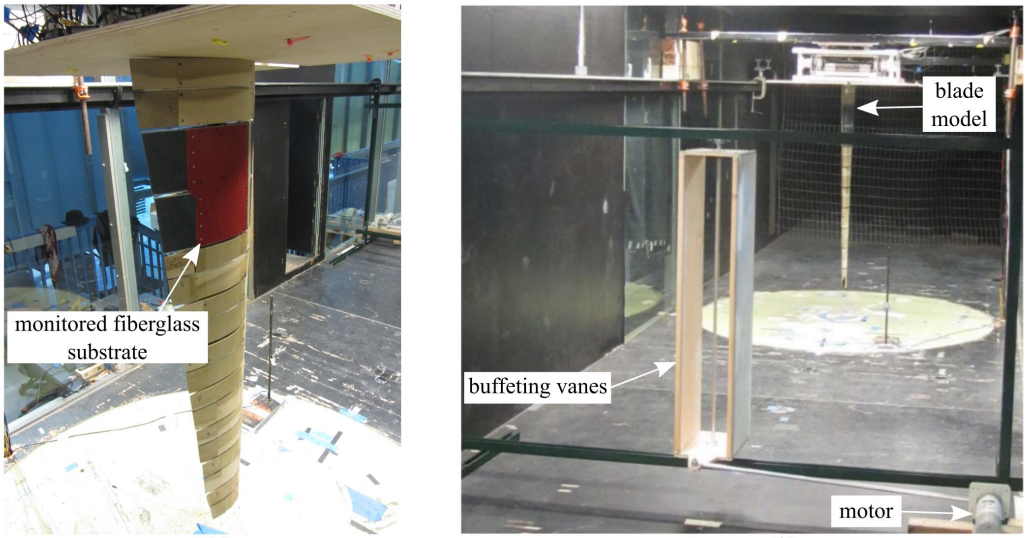

Figure 2. Experimental setup: (a) wind turbine blade mounted in wind tunnel; and (b) buffeting vanes used for generating turbulent airflow.

An HDSN consisting of 12 SECs and 8 RSGs was deployed onto the inside surface of a fiberglass substrate, which was installed onto a wind turbine blade as shown in figure 2(a). The experimental setup consisted of a 1.3-meter blade modeled after the center portion of a full-scale wind turbine blade. The model (figure 2(a)) consisted of an aluminum spar fixed at the root (blade root mounted up) and 10 wood/plastic airfoil sections mounted onto it.[26] The blade root was restrained in all 6 degrees-of-freedom, with root forces monitored via force transducers. Two Transducer Techniques model MDB-50 were used to monitor lift and moment, and an MDB-25 was used to measure drag forces at the root. Lastly, the model was instrumented with 7 accelerometers, PCB model # 352C65, mounted inside the model.

Experimental validation of the vertically mounted model was carried out in the Aerodynamic and Atmospheric Boundary Layer (AABL) wind and gust tunnel located in the Wind Simulation and Testing Laboratory (WiST Lab) in the Department of Aerospace Engineering at Iowa State University. The wind tunnel has an aerodynamic test section of 2.44 m width by 1.83 m height, an atmospheric boundary layer test section of 2.44 m width by 2.21 m height and a design maximum wind speed of 53 m/s in the aerodynamic test section. Air turbulence was induced into the tunnel by forcing the two parallel buffeting vanes shown in figure 2(b) to oscillate at a characteristic frequency of 3.1 Hz. This turbulence created a sinusoidal buffeting load (lift and moment) along the span of the blade.

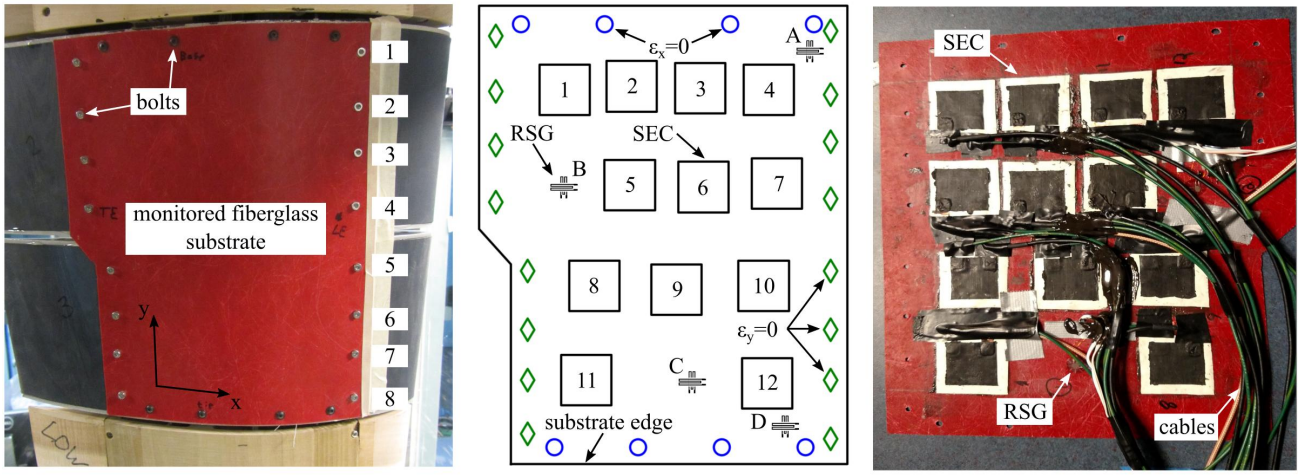

(a) (b) (c)

Figure 3. Experimental HDSN configuration: (a) monitored fiberglass substrate with labeled bolts along the leading edge; (b) schematic with labeled SECs and RSGs; virtual sensors in the x and y directions are denoted by blue circles and green diamonds, respectively; and (c) picture of the HDSN (RSGs A and D not shown, as they were added after the substrate was installed on the model), interior surface view.

The experimental HDSN tested here consisted of 12 3×3 cm^2 SECs and 8 unidirectional RSGs, TML model # FCA-2, mounted on a 0.8 mm-thick fiberglass substrate (figure 3(a)) measuring approximately 270 x 220 mm^2. The fiberglass composite skin was attached to the second and third airfoil sections counted from the blade root. The majority of the bending induced strain developed in the gap between the sections. The deployed HDSN is presented in figure 3(b). Twenty-four bolts were used to fasten the substrate onto the model. Boundary conditions for the bolts were assumed such that $\varepsilon_x = 0$ at each bolt location along the top and bottom of the plate, and $\varepsilon_y = 0$ at each bolt location along the vertical edges of the plate (see figure 3(b)). Figure 3(c) is a picture of the fiberglass panel that was attached to the blade model with 12 SECs and 4 of the 8 RSGs mounted. The remaining 4 RSGs were installed after the substrate was attached to the model. The SEC data acquisition consisted of three custom-built microcontrollers, Atmel P328, each with a 24 bit 4 channel capacitance to digital (CDC) converter sampled at 22 Samples/second (S/s). RSG measurements were obtained using a National Instruments 24-bit 350 Ω quarter-bridge modules (NI-9236) and sampled at 2000 S/s.

Damage was introduced in the form of changing boundary conditions through removing the bolts on the leading edge (facing into the wind flow) of the blade. The removed bolts are annotated in figure 3(a) and their order of removal for 8 different damage cases are listed in Table 1. Unidirectional strain mats are realized for each damage case. Experimental data sets were acquired following the introduction of each damage case, therefore, including the healthy case nine total data sets were acquired.

Table 1. Boundary conditions (bolts) removed for each damage case.

	damage case (no.)							
	1	2	3	4	5	6	7	8
bolts removed	5	4,5	3,4,5	3,4,5,6	3,4,5,6,7	2,3,4,5,6	1,3,4,5,6,7	1,3,4,5,6,7,8

Damage detection and localization through the updating of assumed boundary conditions and monitoring of the error is investigated using damage case 2. Damage case 2 consists of two missing bolts (bolts 4 and 5). We leverage the concept of updating the assumed boundary conditions through taking various combinations of two missing bolts for damage detection and localization. The five possible damage locations investigated are the removal of boundary conditions (bolts) 2 & 3, 3 & 4, 4 & 5, 5 & 6 and 6 & 7. Assumptions containing bolts 1 and 8 were found to be unacceptable due to the complex interaction of plate's edge effects and the assumed shape function, and are therefore excluded from this introductory work. Damage case 2 was selected because it

provided large enough damage to be trackable with the deployed HDSN, while still providing a relatively large search space of five possible damage locations.

Signal interference between the SEC data acquisition system required that only one microcontroller be operating at any given time. Therefore, experimental data for each test condition (healthy and 8 damage cases) was obtained over 3 repeated test runs, each test recording 4 SECs and all eight RSGs. Final experimental data were compiled using the RSG signal as a reference to align the SEC signals for each test case. To reduce sensor noise in the SEC and provide a common time stamp for data analysis, the sensor signals were filtered as follows. A low pass Weibull filter with a cutoff frequency of 5 Hz was applied to remove any high-frequency noise. Next, a principal component analysis (PCA) decomposition was applied on the SEC signals, retaining the first four eigenvalues. Lastly, the SEC and RSG signals were resampled to 100 Hz using a spline interpolation.

4. VALIDATION

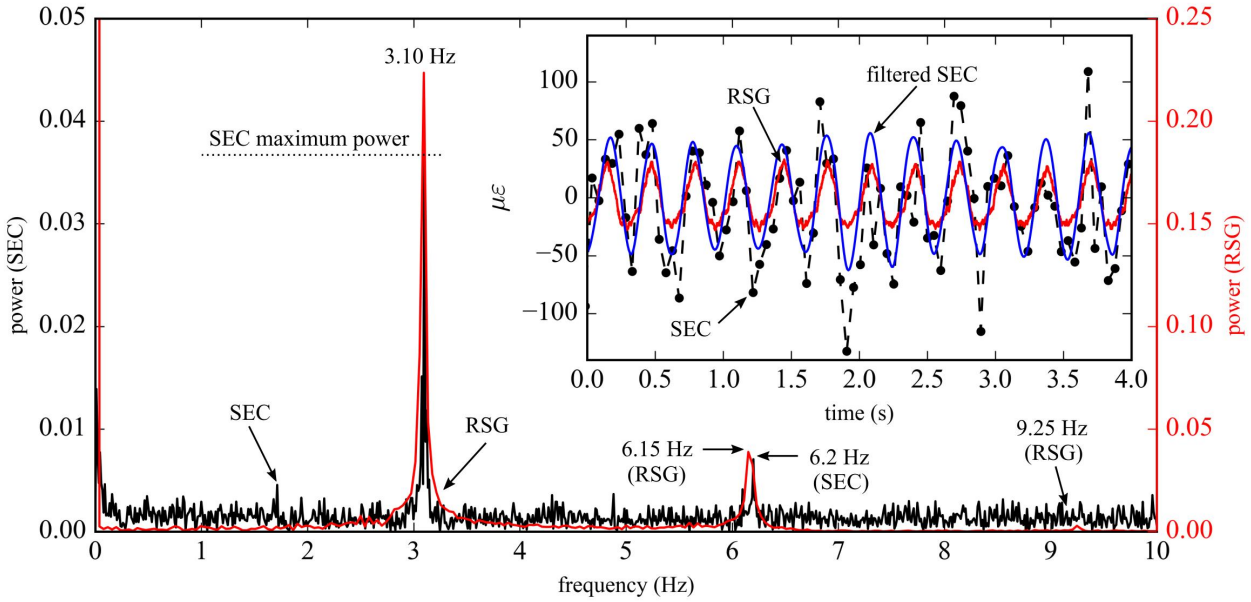

Figure 4. SEC and RSG signals: frequency domain showing the first and second harmonic; (insert) time series data for the SEC and RSG signals.

The capability of the SEC to track the buffeting-induced strain in the wind turbine blade is shown in figure 4. It can be observed that The SEC captures the blade's fundamental frequency at 3.1 Hz and tracks an additional harmonic at 6.2 Hz. Data presented was extracted from SEC #5 and RSG B. A difference of 0.05 Hz is present between the second harmonic detected by the SEC and that of the RSG. A third harmonic is present in the RSG data at 9.25 Hz, but this peak is hardly distinguishable from the SEC's level noise. Given the currents DAQ's low sampling rate of 22Hz, no data past 11Hz is available in the frequency range. Time series data for the SEC and the validating RSG is presented in figure 4(insert). An approximatively sinusoidal shape can be seen in the RSG and SEC data, albeit the SEC was hampered by a much slower sampling rate. Individual SEC strain samples are shown as black dots, and thea filtered SEC signal is presented as the solid blue line. Overall, the SEC exhibit an excellent capability for tracking the blade's response and frequency domain signals while operating in the relatively noisy environment of a wind tunnel.

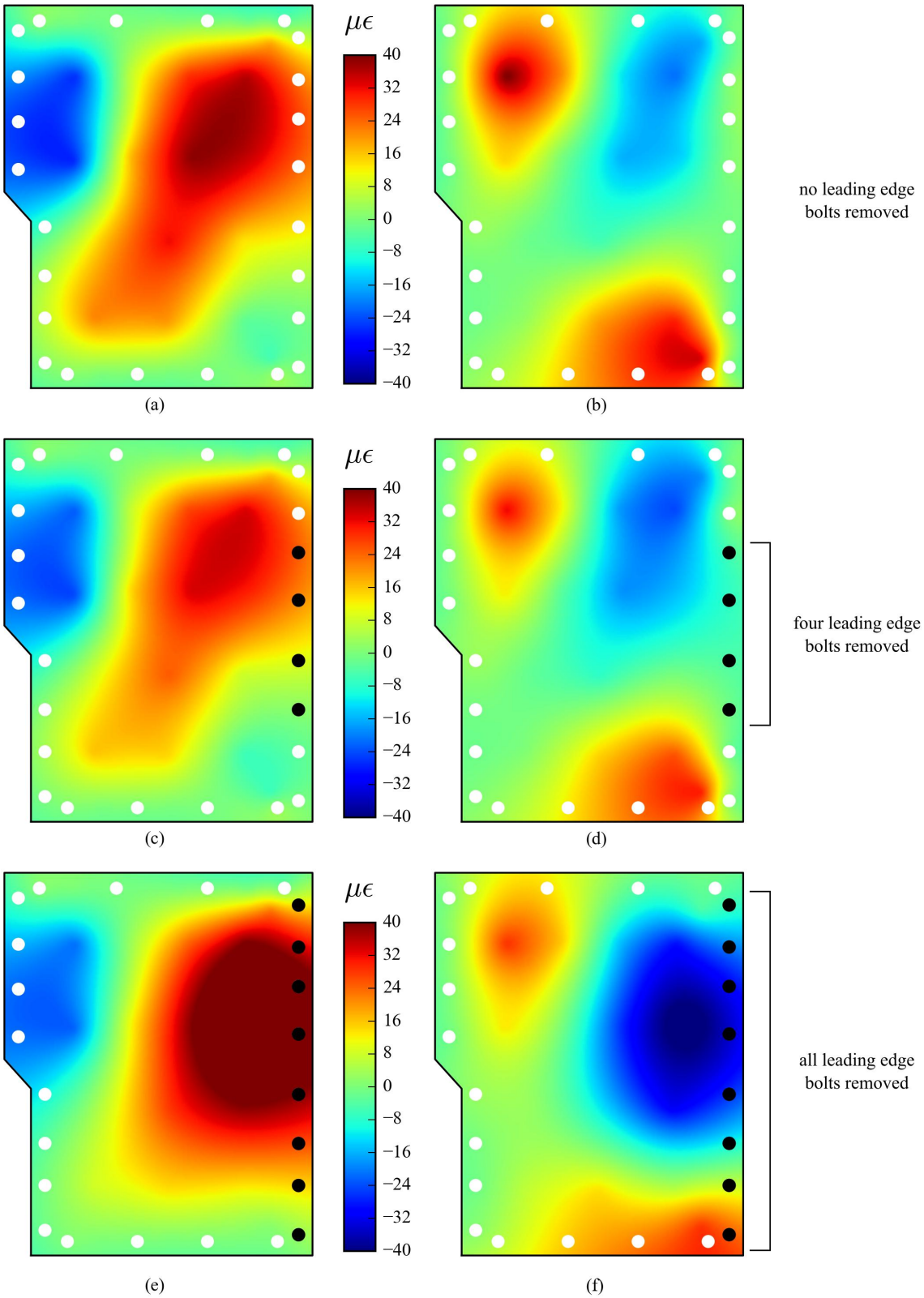

Figure 5. Reconstructed strain maps: (a) healthy condition ε_x; (b) ε_y; (c) damage case 4 ε_x; (d) ε_y; (e) damage case 8 ε_x; (f) ε_y.

The performance of the HDSN as a sensing skin capable of developing full field strain maps in addition to detecting and localizing damage is experimentally validated. Figure 5 shows the decomposed strain maps ε_x and ε_y for the healthy and damage cases 4 and 8. Strain maps are computed from data taken when ε_y at RSG B was at the maximum compressive strain (i.e. when the tip of the model is at its maximum displacement). The reconstructed strain maps for the undamaged test case are presented in figure 5(a-b). The enforced boundary conditions ensure that $\varepsilon_y = 0$ along the leading and trailing edges of the plate. As expected, when bolts are removed for damage cases 4 and 8 and the boundary conditions are updated to reflect the damage, a compressive strain energy moves into the leading edge of the plate. For damage case 8, all leading edge bolts removed, and the majority of the strain energy is present in the middle and along the leading edge of the fiberglass skin that connects the two separate airfoil sections. Additionally, results demonstrates that the HDSN can reconstruct relatively complex strain fields, such as that caused by the torsional motion of the blade model, represented by the different parts of the skin being under tension and compression. The blades torsion detected by the strain maps was corroborated through accelerometers, force transducers, and video captured during testing.

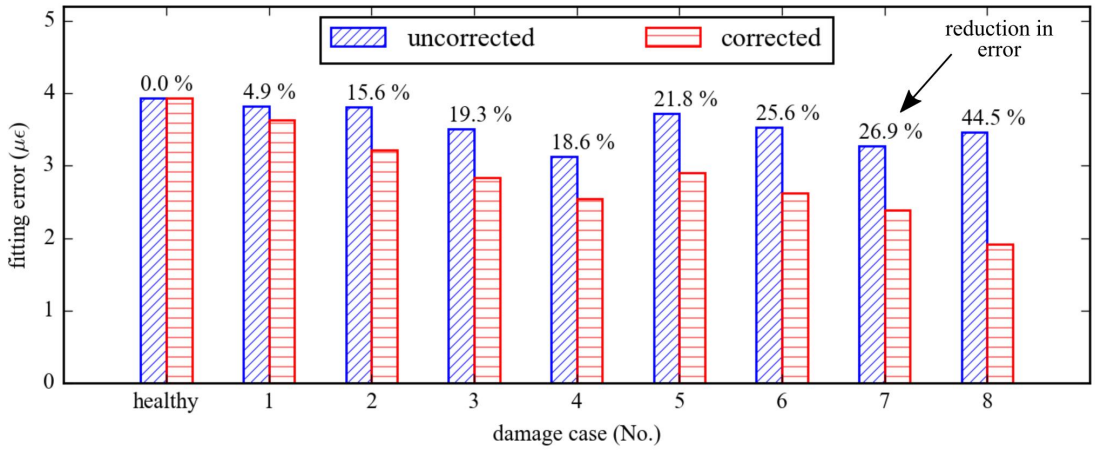

Figure 6. Improvement in strain map reconstruction obtained through the updated of boundary conditions to match the monitored substrate's condition.

Results from updating the enforced boundary conditions to match the damage state of the system is presented in figure 6. Here the error between the estimated strain maps and the experimental RSG data is measured as a mean fitting error across all 8 RSGs for the two orthogonal strain map reconstruction cases. The mean error is obtained by averaging the error throughout six full vibration cycles of the blade model. A comparison in the measured error between uncorrected strain maps that maintain a consistent set of boundary conditions throughout all the damage cases and the corrected strain maps that used an update on the boundary conditions to match each damage case is presented in figure 6. Results demonstrate that updating the boundary conditions to match the damage state provides a consistently better fit than that obtained through the use of static boundary conditions. In the case of damage case 8, a 44.5 % improvement in the measured error is obtained through updating the boundary conditions to match the damage cases. As expected, results demonstrate that updating the boundary conditions to match the damage case results in higher accuracy strain maps.

Experimental data from damage case 2 is used to validate damage detection and localization through leveraging the assumptions on the plate's boundary conditions. Results presented in figure 7 exhibits the fitting error as a function of the boundary conditions that are removed. Boundary conditions were removed in pairs to match the known damage size in damage case 2 (bolts 4 and 5 removed). The fitting error for the removal of bolts 4 and 5 results in a lower fitting error, therefore identifying damage case 2 correctly.

5. CONCLUSION

This paper presented the experimental validation for a novel hybrid dense sensor network (HDSN) for monitoring strain on a wind turbine blade. The HDSN was tested on a scale model of a wind turbine blade in a wind tunnel

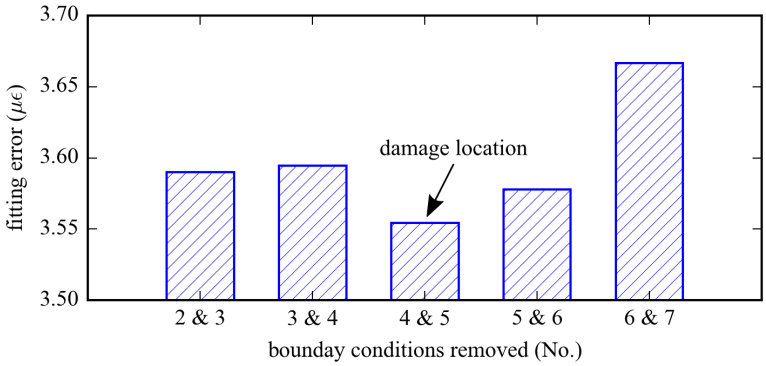

Figure 7. Damage case 2: damage localized through updating the assumed boundary conditions of the plate.

to simulate an operational environment. The HDSN consisted of a large area electronic sensor based on a soft elastomeric capacitor (SEC) combined with resistive strain gauges (RSGs). An extended least squares estimator (LSE)-based algorithm was used to fuse the SEC's additive strain measurements, the RSG's linear strain measurements, and the assumed boundary conditions into unidirectional strain maps. The algorithm assumed a shape function, enforced boundary conditions with the RSG measurements, and used virtual sensors. The regression coefficients were computed using an LSE and used for reconstructing unidirectional strain maps.

Experimental results demonstrated the ability to the HDSN to detect changes in strain maps (i.e. damage) resulting from damage introduced as a change in the monitored substrates boundary conditions. Damage localization is achieved through the updating of the assumed boundary conditions and monitoring the error between reconstructed strain maps and RSG signals. Results showed the promise of the HDSN technology for damage detection along the edge of a monitored area. The HDSN technology and associated damage detection techniques could be used to monitor very large structural components including wind turbine blades. Also, given the demonstrated ability of the HDSN at measuring strain maps, the technology offers potential for updating computational models in real-time. These high fidelity models could then be used for the effective structural health monitoring of structural components or research and development activities. Future work will require an in-depth investigation of the proposed method, including the use of larger HDSN and various types of assumed boundary conditions.

6. ACKNOWLEDGMENTS

The development of the SEC technology was supported by grant No. 13-02 from the Iowa Energy Center. This work is also partly supported by the National Science Foundation Grant No. 1069283, which supports the activities of the Integrative Graduate Education and Research Traineeship (IGERT) in Wind Energy Science, Engineering and Policy (WESEP) at Iowa State University. Their support is gratefully acknowledged.

REFERENCES

1. Svetlana Afanasyeva, Jussi Saari, Martin Kalkofen, Jarmo Partanen, and Olli Pyrhönen. Technical, economic and uncertainty modelling of a wind farm project. *Energy Conversion and Management*, 107:22–33, 2016.
2. Chia Chen Ciang, Jung-Ryul Lee, and Hyung-Joon Bang. Structural health monitoring for a wind turbine system: a review of damage detection methods. *Measurement Science and Technology*, 19(12):122001, 2008.
3. Phillip W. Richards, D. Todd Griffth, and Dewey H. Hodges. Smart loads management for damaged offshore wind turbine blades. *Wind Engineering*, 39(4):419–436, aug 2015.
4. Thommy Ekelund. Yaw control for reduction of structural dynamic loads in wind turbines. *Journal of Wind Engineering and Industrial Aerodynamics*, 85(3):241–262, 2000.

5. Simon Laflamme, Filippo Ubertini, Hussam Saleem, Antonella D'Alessandro, Austin Downey, Halil Ceylan, and Annibale Luigi Materazzi. Dynamic characterization of a soft elastomeric capacitor for structural health monitoring. *Journal of Structural Engineering*, 141(8):04014186, aug 2015.
6. Douglas Adams, Jonathan White, Mark Rumsey, and Charles Farrar. Structural health monitoring of wind turbines: method and application to a hawt. *Wind Energy*, 14(4):603–623, 2011.
7. Yi Zou, LPSG Tong, and Grant P Steven. Vibration-based model-dependent damage (delamination) identification and health monitoring for composite structures-a review. *Journal of Sound and Vibration*, 230(2):357–378, feb 2000.
8. Mark A. Rumsey and Joshua A. Paquette. Structural health monitoring of wind turbine blades. In Wolfgang Ecke, Kara J. Peters, and Norbert G. Meyendorf, editors, *Smart Sensor Phenomena, Technology, Networks, and Systems 2008*. SPIE-Intl Soc Optical Eng, mar 2008.
9. Yong Xu, Fukang Jiang, Scott Newbern, Adam Huang, Chih-Ming Ho, and Yu-Chong Tai. Flexible shear-stress sensor skin and its application to unmanned aerial vehicles. *Sensors and Actuators A: Physical*, 105(3):321–329, aug 2003.
10. Hyung-Kew Lee, Sun-Il Chang, and Euisik Yoon. A flexible polymer tactile sensor: Fabrication and modular expandability for large area deployment. *Journal of Microelectromechanical Systems*, 15(6):1681–1686, dec 2006.
11. Milad Hallaji, Aku Seppänen, and Mohammad Pour-Ghaz. Electrical impedance tomography-based sensing skin for quantitative imaging of damage in concrete. *Smart Materials and Structures*, 23(8):085001, jun 2014.
12. B Yoo, A S Purekar, Y Zhang, and D J Pines. Piezoelectric-paint-based two-dimensional phased sensor arrays for structural health monitoring of thin panels. *Smart Materials and Structures*, 19(7):075017, jun 2010.
13. J. A. Rogers, T. Someya, and Y. Huang. Materials and mechanics for stretchable electronics. *Science*, 327(5973):1603–1607, mar 2010.
14. S-T Tung and B Glisic. Sensing sheet: the response of full-bridge strain sensors to thermal variations for detecting and characterizing cracks. *Measurement Science and Technology*, 27(12):124010, oct 2016.
15. Kenneth J. Loh, Tsung-Chin Hou, Jerome P. Lynch, and Nicholas A. Kotov. Carbon nanotube sensing skins for spatial strain and impact damage identification. *Journal of Nondestructive Evaluation*, 28(1):9–25, mar 2009.
16. Inpil Kang, Mark J Schulz, Jay H Kim, Vesselin Shanov, and Donglu Shi. A carbon nanotube strain sensor for structural health monitoring. *Smart Materials and Structures*, 15(3):737–748, apr 2006.
17. Simon Laflamme, Matthias Kollosche, Jerome J. Connor, and Guggi Kofod. Robust flexible capacitive surface sensor for structural health monitoring applications. *Journal of Engineering Mechanics*, 139(7):879–885, jul 2013.
18. Simon Laflamme, Hussam S. Saleem, Bharath K. Vasan, Randall L. Geiger, Degang Chen, Michael R. Kessler, and Krishna Rajan. Soft elastomeric capacitor network for strain sensing over large surfaces. *IEEE/ASME Transactions on Mechatronics*, 18(6):1647–1654, dec 2013.
19. Hussam Saleem, Austin Downey, Simon Laflamme, Matthias Kollosche, and Filippo Ubertini. Investigation of dynamic properties of a novel capacitive-based sensing skin for nondestructive testing. *Materials Evaluation*, 73(10):1384–1391, oct 2015.
20. Simon Laflamme, Liang Cao, Eleni Chatzi, and Filippo Ubertini. Damage detection and localization from dense network of strain sensors. *Shock and Vibration*, 2016:1–13, 2016.
21. Xiangxiong Kong, Jian Li, Caroline Bennett, William Collins, and Simon Laflamme. Numerical simulation and experimental validation of a large-area capacitive strain sensor for fatigue crack monitoring. *Measurement Science and Technology*, 27(12):124009, oct 2016.
22. Sari Kharroub, Simon Laflamme, Chunhui Song, Daji Qiao, Brent Phares, and Jian Li. Smart sensing skin for detection and localization of fatigue cracks. *Smart Materials and Structures*, 24(6):065004, may 2015.
23. Jingzhe Wu, Chunhui Song, Hussam S Saleem, Austin Downey, and Simon Laflamme. Network of flexible capacitive strain gauges for the reconstruction of surface strain. *Measurement Science and Technology*, 26(5):055103, apr 2015.

24. Austin Downey, Simon Laflamme, and Filippo Ubertini. Reconstruction of in-plane strain maps using hybrid dense sensor network composed of sensing skin. *Measurement Science and Technology*, 27(12):124016, nov 2016.
25. Austin Downey, Chao Hu, and LaFlamme Simon. Optimal sensor placement within a hybrid dense sensor network using an adaptive genetic algorithm with learning gene pool. *Structural Health Monitoring*, In press (2017).
26. Heather Sauder and Partha Sarkar. Aeroelastic model tests of a wind turbine blade for validating load prediction in time domain. In *Proceedings of the 8th International Colloquium on Bluff Body Aerodynamics and Applications*, Boston, MA, June 2016.